Two-step mechanisms in ionization-excitation of He studied by binary $(e,2e)$ experiments and second-Born-approximation calculations

N. Watanabe,[1] M. Takahashi,[1,*] Y. Udagawa,[1] K. A. Kouzakov,[2] and Yu. V. Popov[3]
[1]*Institute of Multidisciplinary Research for Advanced Materials, Tohoku University, Sendai 980-8577, Japan*
[2]*Department of Nuclear Physics and Quantum Theory of Collisions, Faculty of Physics, Moscow State University, Moscow 119992, Russia*
[3]*Nuclear Physics Institute, Moscow State University, Moscow 119992, Russia*
(Received 28 September 2006; revised manuscript received 16 November 2006; published 2 May 2007)

An electron momentum spectroscopy study on ionization-excitation processes of He is reported. The symmetric noncoplanar $(e,2e)$ cross sections for transitions to excited ion states have been measured relative to that to the ground ion state at impact energies of 1240 and 4260 eV. The experimental results exhibit a marked dependence on the impact energy. This provides strong evidence that higher-order effects are involved. Second-Born-approximation calculations are performed and their results are compared with the experimental ones. It is shown that the two-step mechanisms play crucial roles in the ionization-excitation processes.

DOI: 10.1103/PhysRevA.75.052701 PACS number(s): 34.80.Dp

I. INTRODUCTION

Binary $(e,2e)$ spectroscopy, also known as electron momentum spectroscopy (EMS), is an electron-impact ionization experiment at high impact energy and large momentum transfer. Under such high-energy Bethe ridge conditions, it is generally believed that the ionization reaction is dominated by the direct knock-out of the target electron while the residual ion acts as a spectator, as in x-ray Compton scattering. Within the plane wave impulse approximation (PWIA), an ion-recoil-momentum dependent EMS cross section or momentum profile is proportional to the one-electron momentum density of the ionized orbital. Because of its unique advantage of being able to look at electron orbitals in momentum space, EMS has been widely used as a powerful tool for exploring the electronic structure of various systems ([1–5], and references therein).

Helium is one of the most thoroughly explored targets [6–13], since it is simple enough to be a subject of accurate theoretical calculations. Of special interest are simultaneous ionization-excitation processes, i.e., those in which one of the two target electrons is ejected and another is promoted to an empty orbital. Since electron correlation is absent in the one-electron final ion states, electron correlation in the target ground state can be probed directly. In spite of the importance, however, the EMS experiments on the ionization-excitation processes have been hampered by their small cross sections, which are about two orders of magnitude smaller than the cross section for the primary ionization process that leaves the residual He^+ ion in the $n=1$ ground state.

Early EMS studies on ionization-excitation processes of He [8–10] reported the results that can be well interpreted within the first-order theory such as PWIA, which assumes the incident electron to interact with the target only once. The issue of the present paper was raised by a recent study conducted by Lermer *et al.* at an impact energy of 1200 eV [11], where a remarkable intensity difference between experiment and PWIA results has been found in the case of the momentum profile for transition to the $n=2$ excited state of He^+. The experimental $n=2$ results, normalized relative to the momentum profile for the $n=1$ transition, have shown about 35% larger intensity than highly sophisticated PWIA calculations using the Cann and Thakkar wave function [14] and the 141-term Kinoshita-type wave function [15]. Accordingly, Lermer *et al.* [11] suggested the failure of the PWIA description of the binary $(e,2e)$ scattering processes for transitions to excited states of He^+.

More recently we also carried out an EMS study on the ionization-excitation process of He, as well as the double ionization process, at an impact energy of 2080 eV with higher statistical precision [12]. Even at this rather high energy, the experimental $n=2$ momentum profile has been found to exhibit about 25% higher intensity than the PWIA prediction. Furthermore, based on a qualitative analysis of second Born terms made in our previous EMS studies on H_2 [16–18], we have suggested that the two-step (TS) mechanisms [19,20] play crucial roles in the ionization-excitation processes of He as well, resulting in the intensity difference between experiment and PWIA results. Note that after our study [12], Ren *et al.* [13] reported momentum profiles for transitions to the $n=1$, 2, and 3 states of He^+ at impact energies of 1000 and 1600 eV. However, all the momentum profiles were individually normalized to PWIA calculations [21], and consequently the experimental results were employed solely to examine the impact energy dependence of the momentum profiles in terms of shape, not intensity.

The TS mechanisms involve two successive collisions between electrons; ionization-excitation can take place through processes in which one of the two target electrons is ejected due to a binary $(e,2e)$ collision before or after excitation of another electron due to a collision with the incoming or outgoing electrons. As is discussed below, scattering amplitudes associated with the TS mechanisms depend upon impact energy in a way different from that for the PWIA amplitude. Hence a comparison of momentum profiles measured at several impact energies would be helpful for probing the TS mechanisms in the ionization-excitation processes.

*Electronic address: masahiko@tagen.tohoku.ac.jp

Another convincing proof of the footprints of the TS mechanisms in the ionization-excitation processes of He should be given by second-Born-approximation (SBA) calculations. It should be remarked that the SBA method [22–27] has been primarily developed for $(e,2e)$ studies involving a low-energy ejected electron and/or small momentum transfer. A recent such study on ionization-excitation of He conducted by Bellm *et al.* [28] has demonstrated once again, using a hybrid distorted-wave $+R$ matrix (close coupling) with pseudostates approach [29], that treating the projectile-target interaction at least to second order is crucial to obtain reasonable agreement between theory and experiment. However, the kinematics of Bellm *et al.* [28] is far from the high-energy Bethe ridge regime and, accordingly, the EMS conditions. Only recently Dal Cappello *et al.* [30] have used the SBA method to evaluate EMS cross sections for ionization-excitation of H_2. To the best of our knowledge, this is the first calculation of EMS cross sections which incorporate contributions of the TS mechanisms. However, their results have indicated that contributions of the TS mechanisms are not sizable, leaving the observed discrepancies between experiments and PWIA results [16,17] unresolved.

Under these circumstances, we have carried out EMS experiments on He at impact energies of 1240 and 4260 eV using an energy- and momentum-dispersive multichannel $(e,2e)$ spectrometer [17]. We have also performed the SBA calculations. In the present paper, the impact energy dependence of the measured momentum profiles is rigorously investigated. Results of the SBA calculations are compared with those of the experiments for elucidating the roles of the TS mechanisms in the considered processes.

II. EXPERIMENT

EMS is a high-energy electron-impact ionization experiment which involves coincident detection of two outgoing electrons. With the help of the energy and momentum conservation laws, the recoil momentum $\boldsymbol{q}$ of the residual ion and the binding energy E_{bind} of the ejected electron can be determined:

$$\boldsymbol{q} = \boldsymbol{p}_0 - \boldsymbol{p}_1 - \boldsymbol{p}_2 \tag{1}$$

and

$$E_{\mathrm{bind}} = E_0 - E_1 - E_2. \tag{2}$$

Here $\boldsymbol{p}_j$s and E_js $(j=0,1,2)$ are momenta and kinetic energies of the incident and two outgoing electrons, respectively.

In the symmetric noncoplanar geometry two outgoing electrons having equal energies $(E_1=E_2)$ and making equal polar angles $(\theta_1=\theta_2=45°)$ with respect to the incident electron beam axis are detected in coincidence. Then the magnitude of the ion recoil momentum q is expressed by

$$q = \sqrt{(p_0 - \sqrt{2}p_1)^2 + [\sqrt{2}p_1 \sin(\Delta\phi/2)]^2}, \tag{3}$$

where $\Delta\phi$ $(=\phi_2-\phi_1-\pi)$ is the out-of-plane azimuthal angle difference between the two outgoing electrons. If the incident electron energy and momentum are fixed, the ionization transition with binding energy E_{bind} can be simply selected by the choice of the detection energy $(E_1=E_2)$ and the ion recoil momentum q can be determined only by $\Delta\phi$.

In the present work a recently developed $(e,2e)$ spectrometer [17,18] was employed. Briefly, electron impact ionization occurs where an incident electron beam collides with a gaseous He target. Scattered electrons leaving the ionization point are limited by a pair of apertures so that the spherical analyzer accepts those with $\theta_1=\theta_2=45°$ over the azimuthal angle ranges $70° \leqslant \phi_1 \leqslant 110°$ and $250° \leqslant \phi_2 \leqslant 290°$. A rather large acceptance angle of $\Delta\theta=\pm 1.5°$ is used to achieve higher collection efficiency, though it lowers the instrumental energy and momentum resolution. The electrons passing through the apertures are energy analyzed by the spherical analyzer and detected by a pair of position-sensitive detectors.

The EMS experiments on He were carried out at impact energies of 1240 and 4260 eV. A commercially available He gas (Nippon Sanso, >99.99995%) was used. The ambient sample gas pressure was kept at 2.7×10^{-4} Pa during the measurements. The instrumental energy and momentum resolution at 1240 and 4260 eV were 2.4 and 8.1 eV full width at half maximum (FWHM) and about 0.2 and 0.3 a.u. at $q\sim1$ a.u., respectively.

In the analysis of the EMS data, calibration of the collection efficiency was made by using accidental coincidence events, in which electrons must be detected uniformly over the detection areas of the position-sensitive detectors. The validity of this data correction procedure [31] was checked by EMS measurements on Ne at around 1240 and 4260 eV, for which the intensity ratio and shape of the momentum profiles for the $2p^{-1}$ and $2s^{-1}$ ionization are known [32–34]. This ensures the reliability of the experimental momentum profiles for He in both relative magnitude and shape.

III. THEORY

A. Second Born approximation

The first and second Born amplitudes f_{B1} and f_{B2}, for the transition to the final target state $\Phi^f_{(-)}$ can be expressed as

$$f_{B1} = \frac{2}{K^2}\langle\Phi_f^{(-)}(\boldsymbol{p}_2)|\sum_{j=1}^{2}\exp(i\boldsymbol{K}\cdot\boldsymbol{r}_j)|\Phi_i\rangle, \tag{4}$$

$$f_{B2} = -\frac{2}{\pi^2}\lim_{\eta\to0}\sum_{v}\int d\boldsymbol{p}_a \frac{\langle\Phi_f^{(-)}(\boldsymbol{p}_2)|-2+\sum_{j=1}^{2}\exp(i\boldsymbol{K}_f\cdot\boldsymbol{r}_j)|\Phi_v\rangle\langle\Phi_v|-2+\sum_{j=1}^{2}\exp(i\boldsymbol{K}_i\cdot\boldsymbol{r}_j)|\Phi_i\rangle}{[p_a^2-\{p_0^2-2(E_v-E_i)\}-i\eta]K_i^2K_f^2}, \tag{5}$$

with $\boldsymbol{K}_i=\boldsymbol{p}_0-\boldsymbol{p}_a$, $\boldsymbol{K}_f=\boldsymbol{p}_a-\boldsymbol{p}_1$, and $\boldsymbol{K}=\boldsymbol{p}_0-\boldsymbol{p}_1=\boldsymbol{K}_i+\boldsymbol{K}_f$. Here $\boldsymbol{r}_j$s $(j=1,2)$ are spatial coordinates of the target electrons. Φ_i and Φ_v represent the initial and intermediate target states with energies E_i and E_v, respectively.

Due to high energy of the ejected electron in the present experiments ($E_2 \geqslant \sim 600$ eV), only the first-order interaction between the ejected electron and the residual ion is taken into account in the final target state $\Phi^{(-)}_f$. From Eq. (4) we have

$$f_{B1} = f_{\mathrm{SU}} + f_{\mathrm{TS1}}, \tag{6}$$

$$f_{\mathrm{SU}} = \frac{2}{K^2}\sqrt{2}\langle \chi^{(-)}_{p_2} | \exp(i\boldsymbol{K}\cdot\boldsymbol{r}) | \varphi_{f,i}\rangle, \tag{7}$$

$$f_{\mathrm{TS1}} = -\frac{4}{K^2}\sqrt{2}\lim_{\eta\to 0}\sum_u \int d\boldsymbol{p}_b \frac{\langle \chi^{(-)}_{\boldsymbol{p}_2}(\boldsymbol{r}_1)\phi_f(\boldsymbol{r}_2)|V_{12}|\chi^{(+)}_{\boldsymbol{p}_b}(\boldsymbol{r}_1)\phi_u(\boldsymbol{r}_2)\rangle\langle \chi^{(+)}_{\boldsymbol{p}_b}|\exp(i\boldsymbol{K}\cdot\boldsymbol{r})|\varphi_{u,i}\rangle}{p_b^2 - p_2^2 - 2(\varepsilon_f - \varepsilon_u) - i\eta}, \tag{8}$$

with the overlapping integral

$$\varphi_{s,t}(\boldsymbol{r}) = \int \phi^*_s(\boldsymbol{r}')\Phi_t(\boldsymbol{r},\boldsymbol{r}')d\boldsymbol{r}'. \tag{9}$$

Here V_{12} represents the interaction potential between two electrons in the system, ϕ_u is the one-electron orbital of the He^+ ion with energy ε_u, and $\chi^{(\pm)}_{\boldsymbol{p}_b}$ is the continuum distorted-wave with momentum $\boldsymbol{p}_b$ (note that the overlap $\langle \chi^{(\pm)}_{\boldsymbol{p}_b}|\phi_u\rangle$ is negligibly small).

f_{SU} describes the shake-up (SU) mechanism in which the incident electron interacts with and knocks out one of the two target electrons and then the other electron is excited as a result of relaxation of the residual ion due to a sudden change in potential. f_{TS1} represents the so-called two-step 1 (TS1) mechanism [19,20]. The simplest scenario of this mechanism is that one of the $1s$ target electrons is ejected by the first collision with the incident electron and the other $1s$ electron is raised to an excited orbital due to the second collision with the ejected target electron.

f_{B2} describes the so-called two-step 2 (TS2) mechanism. It allows the incident electron to interact with the target twice. Here three types of intermediate target states are possible: (i) with two bound electrons, (ii) with one bound electron and one ejected electron, and (iii) with two ejected electrons. The first and second cases are referred to as the TS21 and TS22 mechanisms throughout this paper and the corresponding scattering amplitudes are denoted as f_{TS21} and f_{TS22}. The third case is neglected because the corresponding contributions are expected to be very small under the present experimental conditions. Thus we have

$$f_{B2} = f_{\mathrm{TS21}} + f_{\mathrm{TS22}}, \tag{10}$$

$$f_{\mathrm{TS21}} = -\frac{2}{\pi^2}\sqrt{2}\lim_{\eta\to 0}\sum_{v'}\int d\boldsymbol{p}_a \frac{\langle \chi^{(-)}_{p_2}|\exp(i\boldsymbol{K}_f\cdot\boldsymbol{r}) - 1|\varphi_{f,v'}\rangle\langle\Phi_{v'}| - 2 + \sum_{j=1}^{2}\exp(i\boldsymbol{K}_i\cdot\boldsymbol{r}_j)|\Phi_i\rangle}{[p_a^2 - \{p_0^2 - 2(E_{v'} - E_i)\} - i\eta]K_i^2K_f^2}, \tag{11}$$

$$f_{\mathrm{TS22}} = -\frac{2}{\pi^2}\sqrt{2}\lim_{\eta\to 0}\sum_u \int d\boldsymbol{p}_a \frac{\langle\phi_f|\exp(i\boldsymbol{K}_f\cdot\boldsymbol{r})|\phi_u\rangle\langle\chi^{(-)}_{p_2}|\exp(i\boldsymbol{K}_i\cdot\boldsymbol{r}) - 1|\varphi_{u,i}\rangle}{[p_a^2 - \{p_0^2 - p_2^2 - 2(\varepsilon_u - E_i)\} - i\eta]K_i^2K_f^2}. \tag{12}$$

The index v' in Eq. (11) represents the state with two bound electrons.

B. Plane wave impulse approximation

When $\chi^{(-)}_{p_2}$ in Eq. (7) is replaced with a plane wave and the impulse approximation [1] is used, f_{SU} is equivalent to the PWIA scattering amplitude. Under the symmetric noncoplanar geometry, the PWIA cross section is given by [1]

$$\frac{d^3\sigma_{\mathrm{PWIA}}}{d\Omega_1 d\Omega_2 dE_1} = \frac{p_1p_2}{p_0}\frac{2\pi\kappa}{\exp(2\pi\kappa) - 1}\frac{4}{K^4}G_f(q), \tag{13}$$

$$G_f(q) = \left|\left(\frac{1}{2\pi}\right)^{3/2}\sqrt{2}\int \phi^*_f(\boldsymbol{r}_1)e^{i\boldsymbol{q}\cdot\boldsymbol{r}_2}\Phi_i(\boldsymbol{r}_1,\boldsymbol{r}_2)d\boldsymbol{r}_1 d\boldsymbol{r}_2\right|^2, \tag{14}$$

where $\kappa = 1/|\boldsymbol{p}_1 - \boldsymbol{p}_2|$. Equation (13) tells one that the PWIA cross section is expressed as a product of kinematical and

TABLE I. Intermediate target states involved in the present SBA calculations.

	Intermediate target state	
He^+ final ion state	He	He^+ (+ ejected electron)
$n=1$		
$1s\ ^2S$	$1s2s\ ^1S$	$2s\ ^2S$, $2p\ ^2P$
$n=2$:		
$2s\ ^2S$	$1s2s\ ^1S$	$1s\ ^2S$, $2p\ ^2P$
$2p\ ^2P$	$1s2p\ ^1P$	$1s\ ^2S$, $2s\ ^2S$
$n=3$:		
$3s\ ^2S$	$1s2s\ ^1S$, $1s3s\ ^1S$	$1s\ ^2S$, $2s\ ^2S$, $2p\ ^2P$, $3p\ ^2P$
$3p\ ^2P$	$1s2p\ ^1P$, $1s3p\ ^1P$	$1s\ ^2S$, $2s\ ^2S$, $2p\ ^2P$, $3s\ ^2S$
$3d\ ^2D$		$1s\ ^2S$

structure factors, i.e., $d^3\sigma/d\Omega_1 d\Omega_2 dE_1 = F_f G_f(q)$. The structure factor $G_f(q)$ is independent of E_0 and is a function of q only. Furthermore, under the present experimental conditions the kinematical factor F_f is practically constant upon variations of q and E_{bind}. It means that within the PWIA the shape and relative intensity of momentum profiles are determined only by $G_f(q)$s.

C. Calculations

We performed the SBA calculations by making two more assumptions. First, we neglected effects of distortion of the incident and outgoing electron waves. Thus, the distorted waves $\chi_{p_b}^{(\pm)}$ were replaced with plane waves and the contributions from the intermediate states $\Phi_{v'} = \Phi_i$ or $\phi_u = \phi_f$, which describe effects of distortion of the incident electron wave [20], were neglected. Secondly, only the intermediate target states tabulated in Table I were considered, since they are expected to make dominant contributions to the scattering amplitudes.

In the SBA calculations f_{SU}, f_{TS1}, and f_{TS22} were obtained using the configuration interaction (CI) wave function of Mitroy *et al.* [35], which reproduces 98.6% of the correlation energy. For evaluating the f_{TS21} amplitude, CI calculations were carried out for both the initial and intermediate target states by means of the general CI code CIV3 [36] in order to describe these states in a consistent manner. The CI wave functions were constructed by the $1s$ Hartree-Fock orbital [37] together with several s and p orbitals optimized for the He $1s^2\ ^1S$ and v' states.

PWIA calculations were carried out using the CI wave function of Mitroy *et al.* [35]. In addition, to examine effects of distortion of the incident and outgoing electron waves, the momentum profiles were calculated using the distorted wave Born approximation (DWBA) method with the aid of the program supplied from McCarthy [38]. In the calculations the static potential of the He ground state and that of the final He^+ ion state were used to produce distorted waves for describing the incident and outgoing electrons. For comparisons with the experiments, all of the SBA, PWIA, and DWBA momentum profiles were folded with the instrumental momentum resolution according to the procedure of Migdall *et al.* [39].

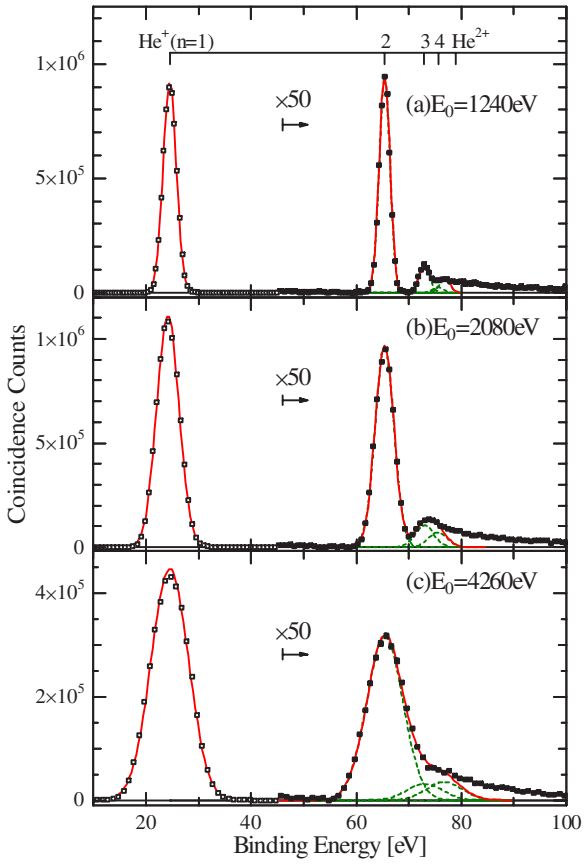

FIG. 1. (Color online) Binding energy spectra of He at $E_0 = 1240$, 2080, and 4260 eV. For ease of comparison, the data responsible for ionization-excitation processes at $E_{\text{bind}} > 45$ eV are scaled by a factor of 50. Deconvoluted curves are shown by broken lines. The solid line represents their sum.

IV. RESULTS

A. Binding energy spectra

In Fig. 1 we show $\Delta\phi$-angle integrated binding energy spectra of He obtained at $E_0 = 1240$ and 4260 eV, together with the spectrum at 2080 eV reported previously [12]. Vertical bars indicate the ionization energies [40], showing the transitions to the $n=1$, 2, and 3 states of He^+ at $E_{\text{bind}} = 24.6$, 65.4, and 73.0 eV, respectively. For ease of comparison the data at $E_{\text{bind}} > 45$ eV are scaled by a factor of 50.

It can be seen from the figure that the instrumental energy resolution does not allow a complete separation of the $n=2$ transition from the adjacent $n=3$ transition at both $E_0 = 2080$ and 4260 eV. However, it is possible to extract contribution of the $n=2$ transition by deconvolution, in which a Gaussian curve with a width of the instrumental energy resolution is assumed for each transition. The results are shown by broken lines and the solid line is their sum. A similar fitting procedure was repeated for a series of binding energy spectra at each azimuthal angle difference or ion recoil momentum. Experimental momentum profiles for the $n=1$ and

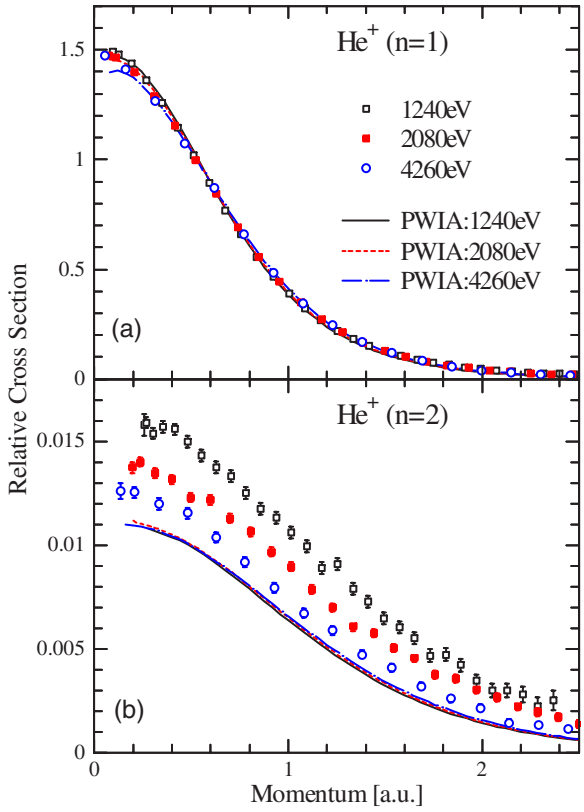

FIG. 2. (Color online) Experimental momentum profiles of He for (a) the $n=1$ transition and (b) the $n=2$ transition at $E_0=1240$, 2080, and 4260 eV. The $n=1$ momentum profiles are individually normalized by setting their areas equal to unity. See text for details.

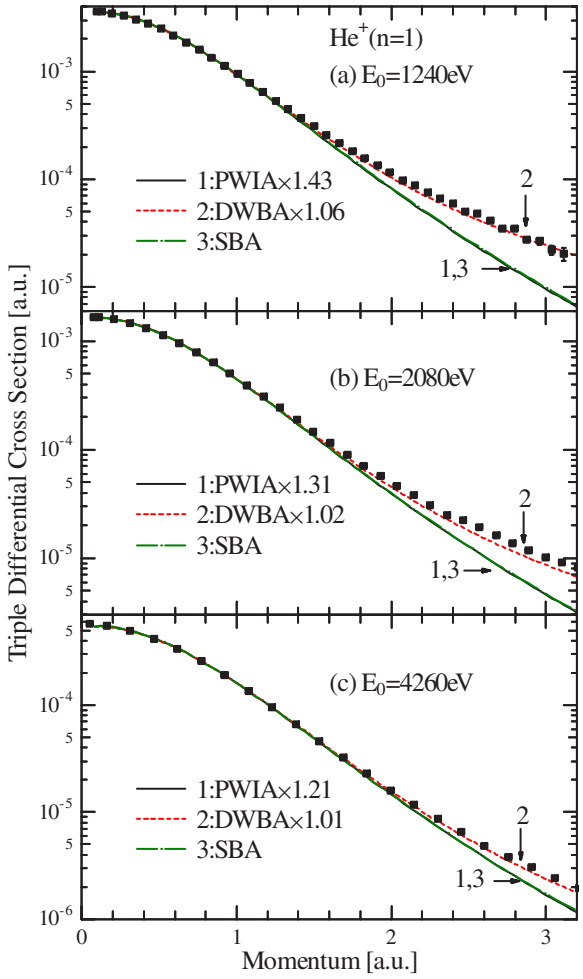

FIG. 3. (Color online) Comparison of experimental and theoretical momentum profiles of He for the $n=1$ transition at $E_0=1240$, 2080, and 4260 eV. All the momentum profiles are shown as a normalized intensity relative to the SBA momentum profiles at individual E_0s. See text for details.

2 transitions were subsequently produced by plotting areas under the corresponding Gaussian curves as a function of the ion recoil momentum. Likewise, the momentum profile for the $n=3$ transition was obtained at $E_0=1240$ eV where a relatively better energy resolution was achieved.

B. Momentum profiles

Although the absolute $(e,2e)$ cross section cannot be determined with EMS, one can examine the experimental momentum profiles for the $n=2$ and 3 transitions in terms of both shape and intensity relative to the $n=1$ cross section. A secure base for such examination is the fact that the relative magnitudes of the momentum profiles for individual transitions are reliable as noted in Sec. II, as well as the findings of the previous EMS studies that the PWIA provides a very good description of the $n=1$ transition [1,5–8,12]. In the present work we use two kinds of normalization procedures for the $n=1$ cross section: one is employed for Fig. 2 and the other for Figs. 3–5 (see below).

Figure 2 shows the experimental $n=1$ and 2 momentum profiles measured at $E_0=1240$, 2080 [12], and 4260 eV, together with the theoretical ones within the PWIA. Here all the $n=1$ results are individually normalized by setting their areas in a momentum range of $0.1<q<1.7$ a.u. equal to unity. The normalization factors used for the $n=1$ results are applied to the corresponding $n=2$ momentum profiles. Hence all the $n=2$ momentum profiles are placed on a common intensity scale, relative to the normalized $n=1$ momentum profiles. It should be pointed out that the PWIA $n=1$ and 2 momentum profiles vary little in shape with the impact energy, even if they are folded with the instrumental momentum resolution which is a function of E_0. The observation strongly suggests that the experimental results are affected by the momentum resolution in a similar fashion. This fairly well justifies the employed normalization procedure which aims at clarifying experimentally whether or not the PWIA is valid for the $n=2$ transition at the examined impact energy values.

On the other hand, in Figs. 3 and 4, the experimental $n=1$ and 2 momentum profiles are plotted so as to share a common intensity scale with the SBA calculations. This is realized as follows. First, the $n=1$ results at individual impact energies were scaled so that their areas in the momentum range up to $q=1.7$ a.u. become equal to those of the corresponding SBA calculations. The scaling factors obtained for the $n=1$ results were subsequently applied to the

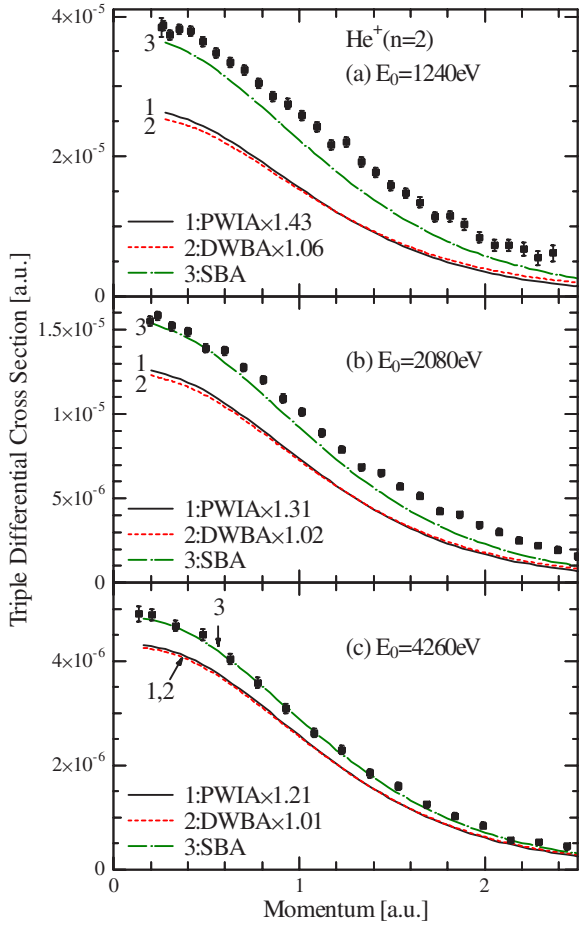

FIG. 4. (Color online) Comparison of experimental and theoretical momentum profiles of He for the $n=2$ transition at $E_0=1240$, 2080, and 4260 eV. All the momentum profiles are shown as a normalized intensity relative to the SBA cross sections for the $n=1$ transition at individual E_0s. See text for details.

$n=2$ results, as well as to the $n=3$ momentum profile at 1240 eV shown in Fig. 5. Note that the $n=2$ and 3 results in Figs. 4 and 5 are plotted on a linear scale, while the $n=1$ results in Fig. 3 are presented on a logarithmic scale in order to make clearly visible the differences between momentum profiles at large momenta where the $(e,2e)$ intensity is relatively small.

Also included in Fig. 3 are the theoretical $n=1$ momentum profiles generated by the PWIA and DWBA calculations. The PWIA (DWBA) results at $E_0=1240$, 2080, and 4260 eV are scaled by factors of 1.43, 1.31, and 1.21 (1.06, 1.02, and 1.01), respectively. Each factor has been obtained so that the area under the momentum profile in the momentum range is the same as that of the corresponding SBA $n=1$ calculations. The $n=2$ and 3 momentum profiles by the PWIA and DWBA methods, shown in Figs. 4 and 5, are scaled by the same factors. This normalization procedure is employed for comparing the experiments with different kinds of theoretical calculations on a common intensity scale, while they are being presented on the basis of the SBA cross sections for the $n=1$ transition.

C. Scattering amplitudes of individual SBA terms

Within the SBA method developed in this work, the total $(e,2e)$ scattering amplitude is given by the sum of the f_{SU}, f_{TS1}, f_{TS21}, and f_{TS22} terms. One of the advantages of the present SBA method is that the terms have their own scattering scenarios and they can be assessed individually. Hence we have calculated their scattering amplitudes for the $n=2$ transition in order to gain deeper insight into dynamics of the ionization-excitation process. The absolute squares $|f_{SU}|^2$, $|f_{TS1}|^2$, $|f_{TS21}|^2$, and $|f_{TS22}|^2$ calculated at $E_0=1240$ eV are plotted in Fig. 6. Note that $|f_{SU}|^2$ is scaled by a factor of 0.3 for ease of comparison.

V. DISCUSSION

A. Impact energy dependence

It is evident from Fig. 2 that the normalized experimental $n=1$ momentum profile does not vary in shape with the change in impact energy. This is consistent with the findings of the previous EMS studies [1,5–8,12] that PWIA provides a very good description of the $n=1$ transition at $E_0>200$ eV. Indeed, the PWIA calculations reproduce the experiments satisfactorily.

On the other hand, for the $n=2$ transition, although the experimental momentum profiles vary little in shape, the experiment clearly shows an impact energy dependence that the PWIA cannot predict. While the PWIA momentum profile remains almost unaltered, the experiment exhibits about 45, 25, and 13 % larger intensity at small momenta than the PWIA prediction at $E_0=1240$, 2080, and 4260 eV, respectively. The reason why the PWIA results are unaltered is due to the fact that the ratio of kinematical factors for the $n=1$ and 2 transitions is always very close to unity: $F_{n=2}/F_{n=1}=0.96$, 0.98, and 0.99 at $E_0=1240$, 2080, and 4260 eV, respectively. Let us recall that relative intensities of the momentum profiles within the PWIA are determined only by structure factors $G_f(q)$s and do not depend upon impact energy. Thus the marked impact energy dependence of the experimental $n=2$ momentum profile provides strong evidence that higher-order approximations beyond the PWIA approach are required.

B. Comparison between experiment and SBA calculations

Two possible improvements over the PWIA description can be conceived: one is effects of the electron wave distortion, and the other is those of the TS mechanisms, which are taken into account in the present DWBA and SBA calculations, respectively. Thus, the importance of these effects can be examined simultaneously.

It can be seen from Fig. 3 that the SBA momentum profile for the $n=1$ transition is indistinguishable from the PWIA results at every examined impact energy value, and that all the theoretical momentum profiles wholly reproduce the experiments. However, one may notice small discrepancy at large momenta; the experimental intensity is a little bit larger than the theoretical prediction. Furthermore, one can see a

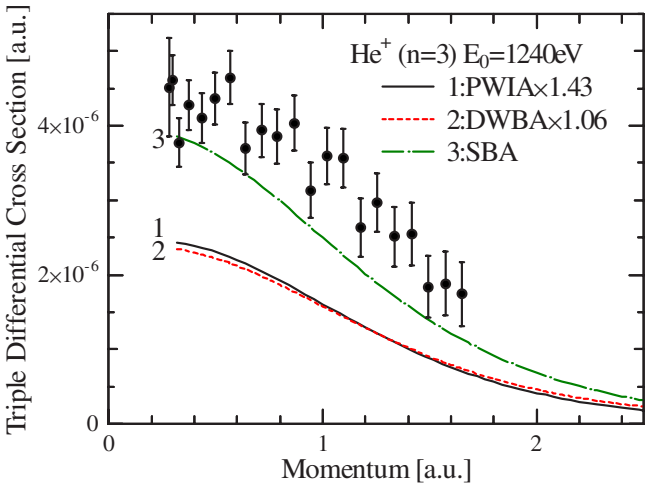

FIG. 5. (Color online) Comparison of experimental and theoretical momentum profiles of He for the $n=3$ transition at $E_0=1240$ eV. All the momentum profiles are shown as a normalized intensity relative to the SBA cross sections for the $n=1$ transition at 1240 eV. See text for details.

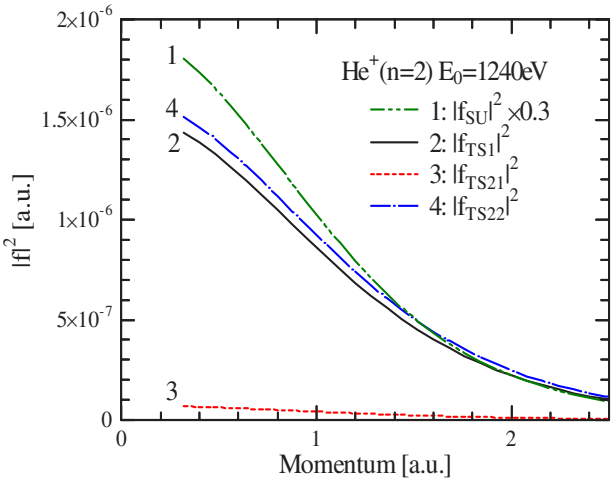

FIG. 6. (Color online) Absolute squares of the scattering amplitudes f_{SU}, f_{TS1}, f_{TS21}, and f_{TS22}, calculated at $E_0=1240$ eV. $|f_{SU}|^2$ is scaled by a factor of 0.3 for ease of comparison.

tendency that the discrepancy becomes less noticeable as the impact energy is higher. Such discrepancy is almost completely resolved by the DWBA method and hence it can be attributed to distorted wave effects.

Similar to the case above, at large momenta, the DWBA method improves the description for the $n=2$ transition when compared with the PWIA. However, it is clear from Fig. 4 that the DWBA results are almost indistinguishable from the PWIA ones when they are plotted on a linear scale and that for every examined impact energy value the $n=2$ experiment exhibits a few tens of % larger intensity at small momenta than the DWBA and PWIA. Thus the intensity difference between experiment and PWIA observed for the $n=2$ transition cannot be attributed to the distorted wave effects only, as opposed to the $n=1$ case.

One can immediately see that the intensity difference is substantially reduced by the SBA calculations. Considerable contributions of the TS mechanisms to the $(e,2e)$ cross section are unambiguously identified for the $n=2$ transition. In particular, at 4260 eV the SBA calculations reproduce the experiments very well. Importance of the TS mechanisms is also evident for the $n=3$ transition (see Fig. 5). While the PWIA and DWBA calculations underestimate the experimental cross section by as much as about 45%, the SBA calculations reduce the deviation from the experiment to about 13%. These observations strongly suggest that the TS mechanisms play important roles not only in ionization excitation but also in other double processes. In fact, for double ionization of He a substantial difference in intensity between experimental and PWIA $(e,3-1e)$ momentum profiles has been found in our previous EMS study at $E_0=2080$ eV [12]. Surprisingly, the experiment has exhibited about three times larger intensity than the PWIA prediction. An extension of our present SBA approach to double ionization of He at large momentum transfer is now in progress.

C. Contributions of individual TS mechanisms

It can be seen from Fig. 6 that intensities of $|f_{TS1}|^2$ and $|f_{TS22}|^2$ are comparable to that of $|f_{SU}|^2$. On the other hand, $|f_{TS21}|^2$ is negligibly small compared with $|f_{TS1}|^2$, $|f_{TS22}|^2$, and $|f_{SU}|^2$. Dominant contributions from f_{TS1} and f_{TS22} over f_{TS21} can be qualitatively understood by considering their simplest scenarios. In the TS1 (TS22) mechanism one of the $1s$ target electrons is ejected by a binary $(e,2e)$ collision with the incident electron, and another target electron is subsequently raised to an excited orbital due to the second collision with the ejected (scattered incident) electron. Note that the projectile energy in the exciting collision is about $E_0/2$. On the other hand, in the TS21 mechanism, the exciting collision occurs before the ionizing $(e,2e)$ collision and hence the projectile energy in the exciting collision is the same as E_0. Thus the observation of dominant contributions from f_{TS1} and f_{TS22} is consistent with the fact that the electron scattering cross section becomes smaller at higher impact energy.

The observation for He is, however, essentially different from that for H_2 reported by Dal Cappello *et al.* [30]. In their calculations, contributions from the f_{TS1} and f_{TS22} terms [defined by Eqs. (14) and (12) in Ref. [30]] are negligibly small, and the most significant second-order contributions are due to the f_{TS21} term [Eq. (10) in Ref. [30]] but are much smaller than the PWIA amplitude. Consequently, the difference between the SBA and PWIA predictions for H_2 is very small and there still exist significant discrepancies between theory and experimental results [16,17]. Further experimental as well as theoretical EMS studies on ionization excitation are thus eagerly awaited.

VI. SUMMARY

We have carried out an EMS study on the ionization-excitation processes of He. Experimentally, the EMS measurements have been performed in the symmetric noncoplanar geometry at impact energies of 1240 and 4260 eV. The $n=2$ momentum profile has been found to exhibit a marked

impact energy dependence, clear evidence that higher-order approximations beyond the first-order PWIA are required. Theoretically, we have made the SBA calculations that incorporate the TS mechanisms. The SBA momentum profiles reproduce well the experimental results at every examined impact energy value. The present work has clarified crucial roles of the TS mechanisms in ionization-excitation processes under the high-energy Bethe ridge conditions.

ACKNOWLEDGMENTS

The authors are grateful to Professor C. Dal Cappello for many fruitful discussions. This research was partially supported by the Ministry of Education, Culture, Sports, Science and Technology, Grant-in-Aid for Scientific Research (A), Grant No. 16205006, and for Exploratory Research, Grant No. 16654065.

[1] I. E. McCarthy and E. Weigold, Phys. Rep., Phys. Lett. **27**, 275 (1976).
[2] C. E. Brion, Int. J. Quantum Chem. **29**, 1397 (1986).
[3] K. T. Leung, in *Theoretical Models of Chemical Bonding*, edited by Z. B. Maksic (Springer-Verlag, Berlin, 1991), Part 3.
[4] M. A. Coplan, J. H. Moore, and J. P. Doering, Rev. Mod. Phys. **66**, 985 (1994).
[5] E. Weigold and I. E. McCarthy, *Electron Momentum Spectroscopy* (Kluwer Academic/Plenum Publishers, New York, 1999).
[6] S. T. Hood, I. E. McCarthy, P. J. O. Teubner, and E. Weigold, Phys. Rev. A **8**, 2494 (1973).
[7] K. T. Leung and C. E. Brion, Chem. Phys. **82**, 87 (1983).
[8] J. P. D. Cook, I. E. McCarthy, A. T. Stelbovics, and E. Weigold, J. Phys. B **17**, 2339 (1984).
[9] A. D. Smith, M. A. Coplan, D. J. Chornay, J. H. Moore, J. A. Tossell, J. Mrozek, V. H. Smith, Jr., and N. S. Chant, J. Phys. B **19**, 969 (1986).
[10] A. Lahmam-Bennani, A. Duguet, C. Dupré, and C. Dal Cappello, J. Electron Spectrosc. Relat. Phenom. **58**, 17 (1992).
[11] N. Lermer, B. R. Todd, N. M. Cann, C. E. Brion, Y. Zheng, S. Chakravorty, and E. R. Davidson, Can. J. Phys. **74**, 748 (1996).
[12] N. Watanabe, Y. Khajuria, M. Takahashi, Y. Udagawa, P. S. Vinitsky, Yu. V. Popov, O. Chuluunbaatar, and K. A. Kouzakov, Phys. Rev. A **72**, 032705 (2005).
[13] X. G. Ren, C. G. Ning, J. K. Deng, G. L. Su, S. F. Zhang, Y. R. Huang, and G. Q. Li, Phys. Rev. A **72**, 042718 (2005).
[14] N. M. Cann and A. J. Thakkar, Phys. Rev. A **46**, 5397 (1992).
[15] T. Kinoshita, Phys. Rev. **105**, 1490 (1957).
[16] M. Takahashi, Y. Khajuria, and Y. Udagawa, Phys. Rev. A **68**, 042710 (2003).
[17] M. Takahashi, N. Watanabe, Y. Khajuria, K. Nakayama, Y. Udagawa, and J. H. D. Eland, J. Electron Spectrosc. Relat. Phenom. **141**, 83 (2004).
[18] M. Takahashi, N. Watanabe, Y. Khajuria, Y. Udagawa, and J. H. D. Eland, Phys. Rev. Lett. **94**, 213202 (2005).
[19] T. A. Carlson and M. O. Krause, Phys. Rev. **140**, 1057 (1965).
[20] R. J. Tweed, Z. Phys. D: At., Mol. Clusters **23**, 309 (1992).
[21] J. K. Deng (private communication).
[22] S. Saxena, K. S. Baliyan, and M. K. Srivastava, J. Phys. B **20**, L611 (1987).
[23] A. Franz and P. L. Altick, J. Phys. B **28**, 4639 (1995).
[24] P. J. Marchalant, C. T. Whelan, and H. R. J. Walters, J. Phys. B **31**, 1141 (1998).
[25] Y. Fang and K. Bartschat, J. Phys. B **34**, L19 (2001).
[26] A. S. Kheifets, Phys. Rev. A **69**, 032712 (2004).
[27] Z. Chen and D. H. Madison, J. Phys. B **38**, 4195 (2005).
[28] S. Bellm, J. Lower, and K. Bartschat, Phys. Rev. Lett. **96**, 223201 (2006).
[29] K. Bartschat and P. G. Burke, J. Phys. B **20**, 3191 (1987).
[30] C. Dal Cappello, A. Mansouri, S. Houamer, and B. Joulakian, J. Phys. B **39**, 2431 (2006).
[31] Y. Miyake, M. Takahashi, N. Watanabe, Y. Khajuria, Y. Udagawa, Y. Sakai, and T. Mukoyama, Phys. Chem. Chem. Phys. **8**, 3022 (2006).
[32] S. W. Braidwood, M. J. Brunger, D. A. Konovalov, and E. Weigold, J. Phys. B **26**, 1655 (1993).
[33] O. Samardzic, S. W. Braidwood, E. Weigold, and M. J. Brunger, Phys. Rev. A **48**, 4390 (1993).
[34] N. Watanabe, Y. Khajuria, M. Takahashi, and Y. Udagawa, J. Electron Spectrosc. Relat. Phenom. **142**, 325 (2005).
[35] J. Mitroy, I. E. McCarthy, and E. Weigold, J. Phys. B **18**, 4149 (1985).
[36] A. Hibbert, Comput. Phys. Commun. **9**, 141 (1975).
[37] E. Clementi and C. Roetti, At. Data Nucl. Data Tables **14**, 177 (1974).
[38] I. E. McCarthy, Aust. J. Phys. **48**, 1 (1995).
[39] J. N. Migdall, M. A. Coplan, D. S. Hench, J. H. Moore, J. A. Tossell, V. H. Smith, Jr., and J. W. Liu, Chem. Phys. **57**, 141 (1981).
[40] A. R. Stringanov and R. S. Svenitskii, *Tables of Spectral Lines of Neutral and Ionized Atoms* (Plenum, New York, 1968).